Progress in Fractional Differentiation and Applications
An International Journal

http://dx.doi.org/10.18576/pfda/120309

Modelling the Impact of Vaccination and Early Detection on the Dynamics of Zika Disease using Atangana-Baleanu-Caputo Fractional Order

John O. Akanni[1,*], *Abayomi A. Ayoade*[2], *Zainab O. Aremu*[3], *and Chinwendu E. Madubueze*[4,5]

[1] Department of Mathematics, School of Engineering, Saveetha Institute of Medical and Technical Sciences, Saveetha University, Chennai 602105, Tamil Nadu, India
[2] Department of Mathematics, University of Lagos, Akoka, Lagos State, Nigeria
[3] Department of Mathematical and Computing Sciences, Koladaisi University, Ibadan, Oyo State, Nigeria
[4] Department of Mathematics, Joseph Sarwuan Tarka University, Makurdi 970101, Benue, Nigeria
[5] Department of Mathematics, Faculty of Science and Technology Universitas Airlangga, Surabaya, Indonesia

Received: 2 May. 2026, Revised: 18 Jun. 2026, Accepted: 20 Jun. 2026
Published online: 1 Jul. 2026

Abstract: This study presents an advanced mathematical model that uses the Atangana-Baleanu-Caputo (ABC) fractional derivative system to investigate Zika virus transmission dynamics. The model incorporates key factors such as vaccination strategies and treatment, offering a more comprehensive understanding of disease spread than traditional models. By applying fractional-order derivatives, the model accounts for extended infection periods, increased population susceptibility, and longer recovery times, leading to prolonged virus transmission. These results emphasise the need for integrated public health strategies that combine vaccination, treatment, and isolation measures to control transmission rates effectively. The fractional-order approach improves the accuracy of disease spread predictions and highlights the importance of sustained control efforts. The virus's persistence is attributed to factors such as slow immune responses, prolonged incubation periods, and treatment-related dynamics. This research provides essential information on Zika virus epidemiology, equipping health authorities and policymakers with tools to refine and optimise control strategies. By integrating memory effects, the model improves its accuracy, providing valuable information for formulating effective disease control strategies.

Keywords: Zika virus, fractional calculus, Atangana-Baleanu-Caputo derivative, epidemic modeling, vaccination strategies, disease transmission dynamics.

1 Introduction

The Zika virus, transmitted primarily by *Aedes* mosquitoes, was first isolated in the Zika Forest of Uganda in 1947 [1] and remained confined to narrow equatorial bands for decades before reaching the Americas during the 2015–2016 outbreak [2]. That outbreak is recalled less for its raw case count than for what followed it: a sharp rise in microcephaly and other congenital neurological abnormalities among infants born to infected mothers [3,4], alongside a smaller but clinically significant burden of Guillain-Barré syndrome in adults [2]. Transmission is not confined to the mosquito-human cycle; the virus also spreads through sexual contact and from mother to fetus [5], which complicates any control strategy built around vector management alone.

Aedes aegypti and *Aedes albopictus*, the principal vectors, are already well established across tropical and subtropical regions [2], and the resulting combination of mosquito-borne and direct human-to-human spread [5] has pushed Zika surveillance past what routine vector-control programmes were designed to handle. This combination of congenital harm, dual transmission routes, and an entrenched vector population [6] makes mathematical modelling of Zika a genuinely open problem rather than a routine reapplication of existing frameworks.

Compartmental models, beginning with the Kermack-McKendrick susceptible-infected-recovered (SIR) formulation [7], remain the standard tool for turning clinical observations of this kind into predictions about spread and control. Since

* Corresponding author e-mail: jide28@gmail.com

© 2026 NSP
Natural Sciences Publishing Cor.

the 2015–2016 outbreak, Zika-specific adaptations of this framework have proliferated [8], folding in mosquito population dynamics, human mobility, and environmental drivers to sharpen predictions for vaccination, vector control, and quarantine strategies. The same compartmental approach has also been applied to infections spread by other mechanical or biological vectors, such as campylobacteriosis carried to food by house flies [9]. Most such models, however, are built on integer-order derivatives, which assume a population's future state depends only on its present state, not its history. Stochastic variants relax the assumption of fixed contact rates [10]. However, neither deterministic nor stochastic integer-order formulations naturally capture the memory effects in which past infections, past interventions, and past environmental conditions continue to shape present transmission that characterizes vector-borne disease dynamics [11].

Fractional-order calculus closes this gap directly. Replacing the integer-order derivative with an operator whose value at time t depends on the entire history of the state variable lets a model capture saturation effects and cumulative dependence on past infections that classical formulations miss [12], and such models have already been applied with some success to malaria, dengue, and Zika transmission alike [13]. Among the available fractional operators, the Atangana-Baleanu derivative, introduced in 2016 [15], is distinguished by its non-singular Mittag-Leffler kernel: unlike the Caputo and Riemann-Liouville operators it generalises, it avoids the singularity $t = \tau$ that can distort short-time behavior while still weighting the full history of the process. In the Caputo sense specifically, this gives the operator a documented advantage for epidemic models in which vector, host, and environmental interactions unfold over the whole course of an outbreak rather than at a single instant [12,16].

Several studies have already applied fractional-order operators to Zika and related mosquito-borne diseases. Zika transmission has previously been modelled with Caputo and ABC-type fractional derivatives incorporating vertical and sexual transmission routes, and comparable ABC formulations have been developed for other vector-borne and co-infection systems, demonstrating the operator's value for capturing memory effects in epidemic recurrence. Those studies, however, do not jointly model vaccination and early detection as coupled control interventions within a seasonally forced mosquito-recruitment framework. The present model addresses this gap by combining a vaccinated compartment (V), an early-detection-linked disease-induced mortality term (δ), and a time-dependent mosquito recruitment function $\Lambda_v(t)$ within a single ABC formulation, which, to the authors' knowledge, has not been jointly examined in prior fractional-order Zika studies [12,17].

Gains attributed to the ABC formulation in these related settings include improved predictive accuracy over classical models [17], a better account of how vector, host, and environmental histories jointly shape transmission [16], and a more faithful representation of the oscillatory or recurrent prevalence patterns that seasonal mosquito populations tend to produce [12]. These are exactly the features a Zika model needs if it has to represent vaccination and early detection as interventions rather than fixed parameters.

This paper focuses on two interventions: vaccination and early case detection, and each has a distinct mathematical signature. A vaccination campaign depletes the susceptible pool directly, which optimal-control formulations of epidemic models make explicit [18]; early detection acts differently, shortening the window in which an infected individual can transmit before isolation [19]. Vaccine models for malaria and dengue point the same way, and add that imperfect protection and waning immunity limit what coverage alone can achieve [20,21]. Fractional-order formulations allow both effects to be modelled with the delay and memory built-in: the cumulative, rather than instantaneous, impact of a vaccination or detection programme can be represented directly in the derivative itself [22], and the same structure credits early detection with preventing onward transmission before it happens rather than only after the fact [23].

Jointly, these tools allow a model to be used, not just to describe an epidemic but to ask when, and at what level to deploy an intervention [24]. When intervention costs are included, the same optimal control framework identifies the most cost-effective combination of measures, as shown for Ebola virus disease and for illicit drug use and banditry [25,26].

The model developed in this paper combines these elements directly: an Atangana-Baleanu-Caputo fractional derivative, a vaccinated compartment, and a detection-linked, disease-induced mortality term, applied to Zika transmission between human and mosquito populations under seasonally forced mosquito recruitment. Section 2 formulates the integer-order model as a baseline, and Section 3 analyses it: positivity and boundedness, the basic reproduction number, the endemic equilibrium, the vaccination threshold, and the sensitivity of R_0. Section 4 extends the model to the ABC operator, establishes the existence of a solution, and derives a semi-analytical solution. Section 5 reports the numerical results and their implications for vaccination and detection policy, and Section 6 concludes. Section 1.1 recalls the fractional-calculus preliminaries used throughout.

1.1 Preliminaries

This section discusses the fundamentals of fractional calculus [14] used later in the work.

Basic 1: For a given function $y(\theta)$ such that $y(\theta) \in Z(a,b)$ with $\Delta \in [0,1]$ and $a > b$, where the order $a > 0$, the ABC differential is defined as:

© 2026 NSP
Natural Sciences Publishing Cor.

$$ {}^{ABC}_{a}D^{a}_{t}y(\theta) = \frac{M(a)}{1-a}\int_{a}^{\tau}\frac{dy(\Delta)}{d\Delta}F_a\left[-\frac{a}{1-a}(\eta-\Delta)^a\right]d\Delta. $$

In which the normalization function is $M(a) = (1-a) + \frac{a}{\Gamma(a)}$, and $F_a(\bullet)$ is the Mittag-Leffler function for $i-1 < a \leq i$, where $i \in \mathbb{M}$ and $y \in C^{i-1}[0,\eta]$.

Basic 2: The ABC integral operator of order $a > 0$ is defined as:

$$ {}^{ABC}D^{\varphi}_{t}(y(a)) = \frac{1-a}{M(a)} + \frac{a}{M(a)\Gamma(a)}\int_{a}^{t} g(\Delta)(\eta-\Delta)^{a-1}d\Delta. $$

Basic 3: The fractional derivative $0 < a \leq 1$ of the Laplace transform for ABC is:

$$ L\left\{{}^{ABC}_{0}D^{a}y(t)\right\}(s) = \frac{M(a)}{1-a}\frac{s^aL\{y(t)s\} - s^{a-1}y(a)}{s^a + \frac{a}{1-a}}. $$

Basic 4: The Adomian polynomials $\alpha_0, \alpha_1, \ldots, \alpha_n$ are applied to decompose an unknown function $W(t) = W_0 + W_1 + W_2 + \ldots + W_n$, and are given by:

$$ \psi_{\varphi} = \frac{1}{u}\frac{d^{\varphi}}{d\Delta^{\varphi}}\left[X(t)\sum_{\alpha=0}^{\varphi}W_{\varphi}\Delta^{\varphi}\right]_{\Delta=0}. $$

Note on notation: the fractional order is denoted a in Basic 1–Basic 4 above, following the general definition; from Equation (3) onward it is written α (matching all figure legends) and, in Section 4's integral equations, ϖ. All three symbols denote the same fractional order throughout this paper.

2 Model Formulation

We develop a deterministic compartmental model to investigate Zika virus transmission dynamics, including interactions between human hosts and mosquito vectors. The model stratifies the total human population N into five epidemiological compartments: susceptible (S), exposed (E), infectious (I), recovered (R), and vaccinated (V). Susceptible individuals (S) are recruited at a rate Π and may acquire infection following bites from infectious mosquitoes (I_v), with the force of infection defined by the term $\beta S\frac{I_v}{N_v}$, where β is the transmission rate from mosquito to human. Exposed individuals (E) progress to the infectious class (I) at a rate σ, while infectious individuals recover at rate γ. A proportion of the susceptible population is vaccinated at rate ν, transferring individuals directly to the vaccinated class (V). All human compartments are subject to natural death at rate μ.

The mosquito vector population N_v is subdivided into three compartments: susceptible (S_v), exposed (E_v), and infectious (I_v). Susceptible mosquitoes (S_v) become infected after biting infectious humans (I), governed by the transmission parameter β_v. Exposed mosquitoes (E_v) progress to the infectious stage (I_v) at rate σ_v. Mosquitoes are recruited into the susceptible class through a time-dependent seasonal recruitment function $\Lambda_v(t)$, which captures climatic and ecological effects on vector population dynamics. All mosquito classes experience natural mortality at rate μ_v, and as mosquitoes do not recover, they remain infectious until death.

The model captures bidirectional transmission: infectious mosquitoes contribute to human infections, and infectious humans contribute to mosquito infections. Incorporating both exposed and vaccinated compartments increases the model's biological realism and provides a robust framework for evaluating control strategies such as vaccination campaigns and vector control interventions. Including seasonal variation in mosquito recruitment allows the model to simulate fluctuating transmission patterns typically observed in tropical endemic regions. The system of equations in Equation (1) describes the model structure and dynamics, with a corresponding schematic representation in Figure 1. Table 1 and Table 2 detail all variables and parameters used in the model, respectively.

Model Equations

$$ \frac{dS}{dt} = \Pi - \beta S\frac{I_v}{N_v} - (\nu+\mu)S $$
$$ \frac{dE}{dt} = \beta S\frac{I_v}{N_v} - (\sigma+\mu+\delta)E $$

© 2026 NSP
Natural Sciences Publishing Cor.

$$\begin{aligned}
\frac{dI}{dt} &= \sigma E - (\gamma + \mu + \delta)I \\
\frac{dR}{dt} &= \gamma I - \mu R \\
\frac{dV}{dt} &= \nu S - \mu V \\
\frac{dS_v}{dt} &= \Lambda_v(t) - \beta_v S_v \frac{I}{N} - \mu_v S_v \\
\frac{dE_v}{dt} &= \beta_v S_v \frac{I}{N} - (\sigma_v + \mu_v)E_v \\
\frac{dI_v}{dt} &= \sigma_v E_v - \mu_v I_v
\end{aligned} \tag{1}$$

Table 1: State variables used in model (1).

Symbol	Description
S	Susceptible humans
E	Exposed (latent) humans
I	Infectious humans
R	Recovered (immune) humans
V	Vaccinated humans
S_v	Susceptible mosquitoes
E_v	Exposed (infected but not yet infectious) mosquitoes
I_v	Infectious mosquitoes
N	Total human population ($N = S+E+I+R+V$)
N_v	Total mosquito population ($N_v = S_v+E_v+I_v$)

Table 2: Model parameters used in model (1).

Parameter	Description
Π	Human recruitment rate
β	Transmission rate from infectious mosquitoes to humans
β_v	Transmission rate from infectious humans to mosquitoes
σ	Rate of progression from exposed to infectious in humans
σ_v	Rate of progression from exposed to infectious in mosquitoes
γ	Recovery rate of infectious humans
ν	Vaccination rate of susceptible humans
μ	Natural mortality rate of humans
δ	Disease-induced mortality rate of humans
μ_v	Natural mortality rate of mosquitoes
Λ_v	Mosquito recruitment rate

3 Model Analysis

This study presents a mathematical model to investigate Zika virus transmission dynamics and incorporate human-mosquito interactions. We perform a qualitative analysis to examine the existence and stability of the disease-free equilibrium, determine threshold conditions for disease invasion, and assess the impact of vaccination. Additionally, we conduct a sensitivity analysis to identify key parameters that influence the basic reproduction number and the disease dynamics.

3.1 Positivity and Boundedness of the Model

To ensure biological relevance and mathematical consistency of model (1), we examine two properties: *positivity*, which ensures non-negative compartments, and *boundedness*, which ensures finite population sizes over time.

© 2026 NSP
Natural Sciences Publishing Cor.

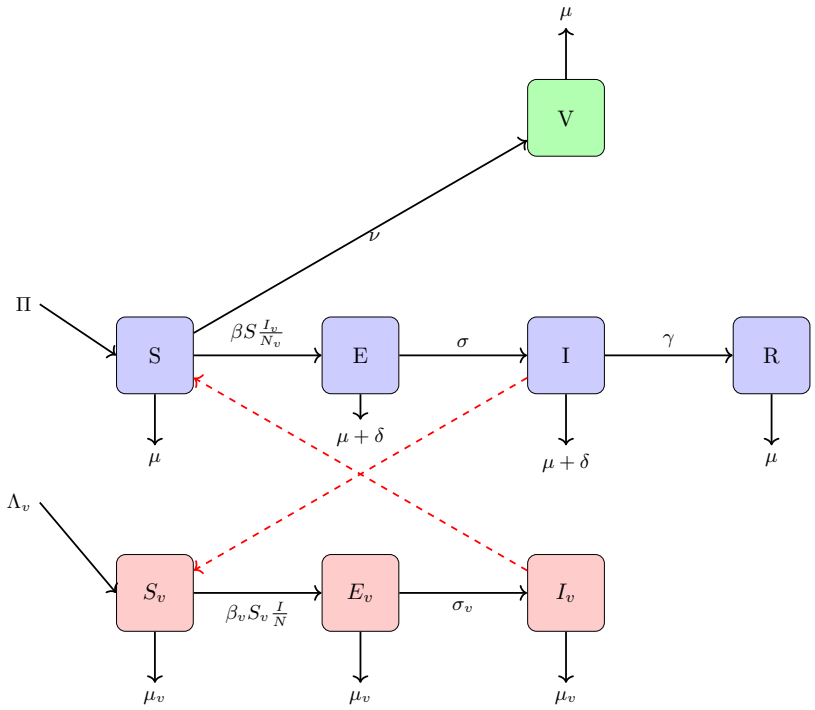


Fig. 1: Flow diagram of the model with demographic processes and mosquito recruitment.

Positivity of Solutions

The Zika virus model ensures biological relevance by confirming two key properties: positivity and boundedness. Positivity guarantees that all compartments (human and mosquito) remain non-negative over time, while boundedness ensures that both human and mosquito populations stay finite.

Positivity is shown by considering the human compartments:

$$\frac{dS}{dt} = \Pi - \beta S\frac{I_v}{N_v} - \nu S - \mu S \geq 0$$

which ensures $S(t) \geq 0$ for all $t \geq 0$.

For boundedness, the total human population $N(t) = S + E + I + R + V$ is bounded above by:

$$N(t) \leq \frac{\Pi}{\mu}, \quad \forall t \geq 0$$

Similarly, for the mosquito population $N_v(t) = S_v + E_v + I_v$, we have:

$$\frac{dN_v}{dt} = \Lambda_v - \mu_v N_v$$

and

$$N_v(t) \leq \frac{\Lambda_v}{\mu_v}$$

These results confirm the model's mathematical consistency and biological realism, supporting its use for theoretical and numerical analysis of Zika virus transmission and control.

3.2 Basic Reproduction Number R_0

The disease-free equilibrium (DFE) represents a state in which no infection is present in the population. The stability of the DFE, determined by the basic reproduction number R_0, helps assess the Zika virus's potential to invade and persist.

© 2026 NSP
Natural Sciences Publishing Cor.

DFE corresponds to a state without infection in human or mosquito populations. In this model for the Zika virus, the DFE is derived by setting the time derivatives of all compartments to zero, resulting in the following conditions:

$$E^0 = I^0 = R^0 = E_v^0 = I_v^0 = 0$$

The equilibrium dynamics for the susceptible and vaccinated human populations are:

$$S^0 = \frac{\Pi}{\nu+\mu} \quad \text{and} \quad V^0 = \frac{\nu\Pi}{\mu(\nu+\mu)}$$

For the mosquito population, the equation for susceptible mosquitoes at equilibrium becomes:

$$S_v^0 = \frac{\Lambda_0}{\mu_v}$$

This reflects a state in which the human population consists of susceptible and vaccinated individuals, and the mosquito population is entirely susceptible, serving as a reference for stability analysis and R_0 calculation.

The basic reproduction number, denoted R_0, is a fundamental threshold parameter in infectious disease modelling. It represents the expected number of secondary infections produced by a single infectious individual in an otherwise entirely susceptible population. The value of R_0 helps determine whether an infectious disease can invade and persist. If $R_0 < 1$, the infection dies out; if $R_0 > 1$, the disease may spread and become endemic.

The expected number of new human infections generated by one infectious mosquito is:

$$R_{mh} = \frac{\beta\Pi\sigma\mu_v}{\Lambda_0(\nu+\mu)(\sigma+\mu+\delta)(\gamma+\mu+\delta)}$$

The expected number of new mosquito infections generated by one infectious human is:

$$R_{hm} = \frac{\beta_v\Lambda_0\sigma_v\mu}{\Pi\mu_v^2(\sigma_v+\mu_v)}$$

The basic reproduction number R_0 is the geometric mean of R_{mh} and R_{hm}:

$$R_0 = \sqrt{R_{mh}\cdot R_{hm}}$$

Substituting the expressions for R_{mh} and R_{hm} into this, we get:

$$R_0 = \sqrt{\frac{\beta\beta_v\mu\sigma\sigma_v}{(\nu+\mu)(\sigma+\mu+\delta)(\gamma+\mu+\delta)(\sigma_v+\mu_v)\mu_v}}$$

Equation R_0 highlights the key biological parameters influencing disease transmission. The transmission coefficients β and β_v, progression rates σ and σ_v, and mortality rates all contribute directly to R_0. Vaccination reduces R_0 because it appears in the denominator. The square root structure reflects the cyclical nature of transmission between hosts and vectors. When $R_0 < 1$, the disease-free equilibrium is locally asymptotically stable, indicating that the disease will eventually die out in the population.

3.3 Endemic Equilibrium

In addition to the disease-free equilibrium, the SEIRV–SEI model admits an *endemic equilibrium* (EE) at which infection persists in both the human and mosquito populations. This equilibrium exists and is biologically feasible if and only if the basic reproduction number satisfies.

$$R_0 > 1.$$

The equilibrium values for the human compartments are:

$$S^* = \frac{\mu N}{(\nu+\mu)R_0}, \quad E^* = \frac{\gamma+\mu+\delta}{\sigma}I^*, \quad I^* = \frac{\sigma(\nu+\mu)}{(\sigma+\mu+\delta)(\gamma+\mu+\delta)}(R_0-1),$$

$$R^* = \frac{\gamma}{\mu}I^*, \quad V^* = \frac{\nu}{\mu}S^*,$$

© 2026 NSP
Natural Sciences Publishing Cor.

where I^* represents the endemic prevalence of infectious humans, R^* is the number of recovered humans, and V^* is the number of vaccinated humans.

For the mosquito population, the equilibrium values are:

$$S_v^* = \frac{\Lambda_v}{\mu_v + \kappa(R_0 - 1)}, \quad E_v^* = \frac{\beta_v S_v^*}{N(\sigma_v + \mu_v)} I^*, \quad I_v^* = \frac{\beta_v S_v^* \sigma_v}{N\mu_v(\sigma_v + \mu_v)} I^*,$$

where κ is a parameter reflecting the interaction between the human and mosquito populations.

These equations describe the long-term persistence of Zika virus when $R_0 > 1$, with all compartments (human and mosquito) at equilibrium. They provide a framework for evaluating the impact of vaccination and vector control strategies on disease prevalence.

3.4 Vaccination Threshold Analysis

Vaccination remains one of the most effective strategies for controlling infectious diseases, particularly in endemic regions where vector control alone may not suffice. A key objective in vaccination modelling is to determine the *critical vaccination threshold*; the minimum proportion of the population that must be immunised to interrupt disease transmission. This threshold corresponds to the condition under which the effective reproduction number, R_e, falls below one. These findings are consistent with established theoretical models and recent research on herd immunity thresholds, emphasising the critical role of the vaccination threshold $\nu_c = \mu(R_0 - 1)$ in disease control.

The effective reproduction number R_e is given by:

$$R_e = R_0 \cdot (1 - p_v),$$

where p_v is the proportion of the human population vaccinated at equilibrium. The proportion vaccinated is:

$$p_v = \frac{\nu}{\nu + \mu}.$$

To prevent the establishment of Zika virus in the population, we require $R_e < 1$, which gives the threshold condition:

$$\nu > \mu(R_0 - 1).$$

The critical vaccination coverage required to achieve herd immunity and prevent Zika outbreaks is:

$$p_v^{\text{crit}} = 1 - \frac{1}{R_0}.$$

This relationship shows that the higher the basic reproduction number R_0, the greater the vaccination coverage required to control the disease. For example, with $R_0 = 3$, at least 66.7% of the population must be vaccinated; for $R_0 = 5$, the threshold increases to 80%.

3.5 Sensitivity Analysis of R_0

Sensitivity analysis of R_0 identifies key parameters affecting disease dynamics, guiding targeted interventions and evidence-based public health decisions, particularly in vaccination policy and disease control.

The normalised sensitivity index quantifies how parameter changes proportionally affect R_0. It is defined mathematically as:

$$\Upsilon_x^{R_0} = \frac{\partial R_0}{\partial x} \cdot \frac{x}{R_0}. \tag{2}$$

The index shows the proportional impact of parameters on R_0; positive values amplify transmission, while negative values reduce it, guiding policy focus. Table 3 lists the sign of the index for each parameter.

© 2026 NSP
Natural Sciences Publishing Cor.

Table 3: Sensitivity analysis of $\mathscr{R}_0$.

Parameter	Sensitivity index
β	+ve
β_v	+ve
μ_v	−ve
σ_v	+ve
γ	−ve
μ	−ve
ν	−ve
δ	−ve
σ	+ve

4 Fractional Zika Virus Fever Model Analysis with the Atangana–Baleanu Operator (ABC)

The Zika virus model is formulated using the Atangana-Baleanu fractional derivative of order α to account for memory effects in both human and mosquito populations. The fractional dynamics of the system are described by:

$$\begin{aligned}
D_t^\alpha S &= \Pi - \beta S\frac{I_v}{N_v} - (\nu+\mu)S \\
D_t^\alpha E &= \beta S\frac{I_v}{N_v} - (\sigma+\mu+\delta)E \\
D_t^\alpha I &= \sigma E - (\gamma+\mu+\delta)I \\
D_t^\alpha R &= \gamma I - \mu R \\
D_t^\alpha V &= \nu S - \mu V \\
D_t^\alpha S_v &= \Lambda_v(t) - \beta_v S_v\frac{I}{N} - \mu_v S_v \\
D_t^\alpha E_v &= \beta_v S_v\frac{I}{N} - (\sigma_v+\mu_v)E_v \\
D_t^\alpha I_v &= \sigma_v E_v - \mu_v I_v
\end{aligned} \tag{3}$$

where D_t^α is the Atangana–Baleanu–Caputo fractional derivative of order α $(0<\alpha<1)$, defined as

$$D_t^\alpha f(t) = \frac{M(\alpha)}{1-\alpha}\int_0^t f'(\tau)E_\alpha\left[-\frac{\alpha}{1-\alpha}(t-\tau)^\alpha\right]d\tau, \tag{4}$$

with $M(\alpha)$ the normalization function defined in Basic 1 and $E_\alpha(\cdot)$ the one-parameter Mittag-Leffler function. This is the operator introduced in Basic 1, and it underlies the Volterra-type equations in (5) below. The derivative D_t^α describes the memory-dependent dynamics of disease transmission. The system includes both human and mosquito compartments, where fractional-order effects influence infection dynamics and model non-local interactions in time. In addition, the initial values are $S(t)=S(0), E(t)=E(0), I(t)=I(0), R(t)=R(0), V(t)=V(0), S_v(t)=S_v(0), E_v(t)=E_v(0), I_v(t)=I_v(0)$.

Throughout the remainder of this section, $\Omega(\varpi)$ denotes the same normalization function $M(\alpha)$ introduced in Basic 1 (Preliminaries), and ϖ denotes the same fractional order α used in Equation (3) and throughout the numerical results (Section 4.2); the symbols are used interchangeably below for consistency with the cited derivation technique.

We now try to apply the volterra-type integral equation to the model (3) which we transformed into ABC as presented below:

$$\begin{aligned}
S(t)-S(0) &= \frac{1-\varpi}{\Omega(\varpi)}\left\{\Pi-\beta S\frac{I_v}{N_v}-\nu S-\mu S\right\}+ \\
&\quad \frac{\varpi}{\Omega(\varpi)\Gamma(\varpi)}\int_0^t\left\{\Pi-\beta S\frac{I_v}{N_v}-\nu S-\mu S\right\}(t-\omega)^{\varpi-1}d\omega, \\
E(t)-E(0) &= \frac{1-\varpi}{\Omega(\varpi)}\left\{\beta S\frac{I_v}{N_v}-\sigma E-\mu E-\delta E\right\}+
\end{aligned}$$

© 2026 NSP
Natural Sciences Publishing Cor.

$$\frac{\varpi}{\Omega(\varpi)\Gamma(\varpi)}\int_0^t\left\{\beta S\frac{I_v}{N_v}-\sigma E-\mu E-\delta E\right\}(t-\omega)^{\varpi-1}d\omega,$$

$$I(t)-I(0)=\frac{1-\varpi}{\Omega(\varpi)}\{\sigma E-\gamma I-\mu I-\delta I\}+\frac{\varpi}{\Omega(\varpi)\Gamma(\varpi)}\int_0^t\{\sigma E-\gamma I-\mu I-\delta I\}(t-\omega)^{\varpi-1}d\omega,$$

$$R(t)-R(0)=\frac{1-\varpi}{\Omega(\varpi)}\{\gamma I-\mu R\}+\frac{\varpi}{\Omega(\varpi)\Gamma(\varpi)}\int_0^t\{\gamma I-\mu R\}(t-\omega)^{\varpi-1}d\omega,$$

$$V(t)-V(0)=\frac{1-\varpi}{\Omega(\varpi)}\{\nu S-\mu V\}+\frac{\varpi}{\Omega(\varpi)\Gamma(\varpi)}\int_0^t\{\nu S-\mu V\}(t-\omega)^{\varpi-1}d\omega,$$

$$S_v(t)-S_v(0)=\frac{1-\varpi}{\Omega(\varpi)}\left\{\Lambda_v(t)-\beta_v S_v\frac{I}{N}-\mu_v S_v\right\}+\frac{\varpi}{\Omega(\varpi)\Gamma(\varpi)}\int_0^t\left\{\Lambda_v(t)-\beta_v S_v\frac{I}{N}-\mu_v S_v\right\}(t-\omega)^{\varpi-1}d\omega,$$

$$E_v(t)-E_v(0)=\frac{1-\varpi}{\Omega(\varpi)}\left\{\beta_v S_v\frac{I}{N}-\sigma_v E_v-\mu_v E_v\right\}+\frac{\varpi}{\Omega(\varpi)\Gamma(\varpi)}\int_0^t\left\{\beta_v S_v\frac{I}{N}-\sigma_v E_v-\mu_v E_v\right\}(t-\omega)^{\varpi-1}d\omega,$$

$$I_v(t)-I_v(0)=\frac{1-\varpi}{\Omega(\varpi)}\{\sigma_v E_v-\mu_v I_v\}+\frac{\varpi}{\Omega(\varpi)\Gamma(\varpi)}\int_0^t\{\sigma_v E_v-\mu_v I_v\}(t-\omega)^{\varpi-1}d\omega. \tag{5}$$

Theorem 4.1. *In Equation (3), the term 'kernels' refers to the components* $\mathbb{A}_1,\mathbb{A}_2,\mathbb{A}_3,\mathbb{A}_4,\mathbb{A}_5,\mathbb{A}_6,\mathbb{A}_7,\mathbb{A}_8$.
The Lipschitz condition and contraction are provided, valid if the following inequality is satisfied:

$$0\le\mathbb{B}_1,\mathbb{B}_2,\mathbb{B}_3,\mathbb{B}_4,\mathbb{B}_5,\mathbb{B}_6,\mathbb{B}_7,\mathbb{B}_8<1$$

Proof. The kernel $\mathbb{A}_1(t,S(t))$ is defined as $\Pi-\beta S\frac{I_v}{N_v}-\nu S-\mu S$.

The kernels $\mathbb{A}_1$ and $\mathbb{A}_2$ are considered functions, such that

$$\|\mathbb{A}_1(t,S_1(t))-\mathbb{A}_1(t,S_2(t))\|=\left\|\Pi-\beta S_1\frac{I_v}{N_v}-\nu S_1-\mu S_1-\Pi-\beta S_2\frac{I_v}{N_v}-\nu S_2-\mu S_2\right\|.$$

$$\left\|-\left(\beta\frac{I_v}{N_v}+\nu+\mu\right)(S_1(t)-S_2(t))\right\|\le\left(\beta\frac{I_v}{N_v}+\nu+\mu\right)\|S_1(t)-S_2(t)\|\le\mathbb{B}_1\|S_1(t)-S_2(t)\|.$$

$$\mathbb{B}_1=\beta\frac{I_v}{N_v}+\nu+\mu,\quad \mathbb{B}_2=(\sigma+\mu+\delta),\quad \mathbb{B}_3=(\gamma+\mu+\delta),$$
$$\mathbb{B}_4=\mu,\quad \mathbb{B}_5=\mu,\quad \mathbb{B}_6=\left(\beta_v\frac{I}{N}+\mu_v\right),$$
$$\mathbb{B}_7=\sigma_v+\mu_v,\quad \mathbb{B}_8=\mu_v.$$

$$\|\mathbb{A}_2(t,E_1(t))-\mathbb{A}_2(t,E_2(t))\|\le\mathbb{B}_2\|E_1(t)-E_2(t)\|,$$
$$\|\mathbb{A}_3(t,I_1(t))-\mathbb{A}_3(t,I_2(t))\|\le\mathbb{B}_3\|I_1(t)-I_2(t)\|,$$
$$\|\mathbb{A}_4(t,R_1(t))-\mathbb{A}_4(t,R_2(t))\|\le\mathbb{B}_4\|R_1(t)-R_2(t)\|,$$
$$\|\mathbb{A}_5(t,V_1(t))-\mathbb{A}_5(t,V_2(t))\|\le\mathbb{B}_5\|V_1(t)-V_2(t)\|,$$

© 2026 NSP
Natural Sciences Publishing Cor.

$$\begin{aligned}
&\|\mathbb{A}_6(t,S_{v1}(t)) - \mathbb{A}_6(t,S_{v2}(t))\| \leq \mathbb{B}_6\|S_{v1}(t) - S_{v2}(t)\|,\\
&\|\mathbb{A}_7(t,E_{v1}(t)) - \mathbb{A}_7(t,E_{v2}(t))\| \leq \mathbb{B}_7\|E_{v1}(t) - E_{v2}(t)\|,\\
&\|\mathbb{A}_8(t,I_{v1}(t)) - \mathbb{A}_8(t,I_{v2}(t))\| \leq \mathbb{B}_8\|I_{v1}(t) - I_{v2}(t)\|.
\end{aligned} \tag{6}$$

Equation (5) is rewritten as

$$\begin{aligned}
S(t) &= S(0) + \frac{1-\varpi}{\Omega(\varpi)}\{\mathbb{A}_1(t,S(t))\} + \frac{\varpi}{\Omega(\varpi)\Gamma(\varpi)}\int_0^t \{\mathbb{A}_1(t,S(t))\}(t-\omega)^{\varpi-1}d\omega,\\
E(t) &= E(0) + \frac{1-\varpi}{\Omega(\varpi)}\{\mathbb{A}_2(t,E(t))\} + \frac{\varpi}{\Omega(\varpi)\Gamma(\varpi)}\int_0^t \{\mathbb{A}_2(t,E(t))\}(t-\omega)^{\varpi-1}d\omega,\\
I(t) &= I(0) + \frac{1-\varpi}{\Omega(\varpi)}\{\mathbb{A}_3(t,I(t))\} + \frac{\varpi}{\Omega(\varpi)\Gamma(\varpi)}\int_0^t \{\mathbb{A}_3(t,I(t))\}(t-\omega)^{\varpi-1}d\omega,\\
R(t) &= R(0) + \frac{1-\varpi}{\Omega(\varpi)}\{\mathbb{A}_4(t,R(t))\} + \frac{\varpi}{\Omega(\varpi)\Gamma(\varpi)}\int_0^t \{\mathbb{A}_4(t,R(t))\}(t-\omega)^{\varpi-1}d\omega,\\
V(t) &= V(0) + \frac{1-\varpi}{\Omega(\varpi)}\{\mathbb{A}_5(t,V(t))\} + \frac{\varpi}{\Omega(\varpi)\Gamma(\varpi)}\int_0^t \{\mathbb{A}_5(t,V(t))\}(t-\omega)^{\varpi-1}d\omega,\\
S_v(t) &= S_v(0) + \frac{1-\varpi}{\Omega(\varpi)}\{\mathbb{A}_6(t,S_v(t))\} + \frac{\varpi}{\Omega(\varpi)\Gamma(\varpi)}\int_0^t \{\mathbb{A}_6(t,S_v(t))\}(t-\omega)^{\varpi-1}d\omega,\\
E_v(t) &= E_v(0) + \frac{1-\varpi}{\Omega(\varpi)}\{\mathbb{A}_7(t,E_v(t))\} + \frac{\varpi}{\Omega(\varpi)\Gamma(\varpi)}\int_0^t \{\mathbb{A}_7(t,E_v(t))\}(t-\omega)^{\varpi-1}d\omega,\\
I_v(t) &= I_v(0) + \frac{1-\varpi}{\Omega(\varpi)}\{\mathbb{A}_8(t,I_v(t))\} + \frac{\varpi}{\Omega(\varpi)\Gamma(\varpi)}\int_0^t \{\mathbb{A}_8(t,I_v(t))\}(t-\omega)^{\varpi-1}d\omega.
\end{aligned} \tag{7}$$

The subsequent recursive formula is:

$$\begin{aligned}
S_n(t) &= S(0) + \frac{1-\varpi}{\Omega(\varpi)}\{\mathbb{A}_1(t,S_{n-1}(t))\} + \frac{\varpi}{\Omega(\varpi)\Gamma(\varpi)}\int_0^t \{\mathbb{A}_1(t,S_{n-1}(t))\}(t-\omega)^{\varpi-1}d\omega,\\
E_n(t) &= E(0) + \frac{1-\varpi}{\Omega(\varpi)}\{\mathbb{A}_2(t,E_{n-1}(t))\} + \frac{\varpi}{\Omega(\varpi)\Gamma(\varpi)}\int_0^t \{\mathbb{A}_2(t,E_{n-1}(t))\}(t-\omega)^{\varpi-1}d\omega,\\
I_n(t) &= I(0) + \frac{1-\varpi}{\Omega(\varpi)}\{\mathbb{A}_3(t,I_{n-1}(t))\} + \frac{\varpi}{\Omega(\varpi)\Gamma(\varpi)}\int_0^t \{\mathbb{A}_3(t,I_n(t))\}(t-\omega)^{\varpi-1}d\omega,\\
R_n(t) &= R(0) + \frac{1-\varpi}{\Omega(\varpi)}\{\mathbb{A}_4(t,R_{n-1}(t))\} + \frac{\varpi}{\Omega(\varpi)\Gamma(\varpi)}\int_0^t \{\mathbb{A}_4(t,R_n(t))\}(t-\omega)^{\varpi-1}d\omega,\\
V_n(t) &= V(0) + \frac{1-\varpi}{\Omega(\varpi)}\{\mathbb{A}_5(t,V_{n-1}(t))\} + \frac{\varpi}{\Omega(\varpi)\Gamma(\varpi)}\int_0^t \{\mathbb{A}_5(t,V_n(t))\}(t-\omega)^{\varpi-1}d\omega,\\
S_{vn}(t) &= S_v(0) + \frac{1-\varpi}{\Omega(\varpi)}\{\mathbb{A}_6(t,S_{vn-1}(t))\} + \frac{\varpi}{\Omega(\varpi)\Gamma(\varpi)}\int_0^t \{\mathbb{A}_6(t,S_{vn}(t))\}(t-\omega)^{\varpi-1}d\omega,\\
E_{vn}(t) &= E_v(0) + \frac{1-\varpi}{\Omega(\varpi)}\{\mathbb{A}_7(t,E_{vn-1}(t))\} + \frac{\varpi}{\Omega(\varpi)\Gamma(\varpi)}\int_0^t \{\mathbb{A}_7(t,E_{vn}(t))\}(t-\omega)^{\varpi-1}d\omega,\\
I_{vn}(t) &= I_v(0) + \frac{1-\varpi}{\Omega(\varpi)}\{\mathbb{A}_8(t,I_{vn-1}(t))\} + \frac{\varpi}{\Omega(\varpi)\Gamma(\varpi)}\int_0^t \{\mathbb{A}_8(t,I_{vn}(t))\}(t-\omega)^{\varpi-1}d\omega.
\end{aligned} \tag{8}$$

The difference between consecutive terms in the following relation:

$$\begin{aligned}
\beth_{1n} &= S_n(t) - S_{n-1}(t) = \frac{1-\varpi}{\Omega(\varpi)}\{\mathbb{A}_1(t,S_{n-1}(t)) - \mathbb{A}_1(t,S_{n-2}(t))\},\\
\beth_{2n} &= E_n(t) - E_{n-1}(t) = \frac{1-\varpi}{\Omega(\varpi)}\{\mathbb{A}_2(t,E_{n-1}(t)) - \mathbb{A}_2(t,E_{n-2}(t))\},\\
\beth_{3n} &= I_n(t) - I_{n-1}(t) = \frac{1-\varpi}{\Omega(\varpi)}\{\mathbb{A}_3(t,I_{n-1}(t)) - \mathbb{A}_3(t,I_{n-2}(t))\},\\
\beth_{4n} &= R_n(t) - R_{n-1}(t) = \frac{1-\varpi}{\Omega(\varpi)}\{\mathbb{A}_4(t,R_{n-1}(t)) - \mathbb{A}_4(t,R_{n-2}(t))\},
\end{aligned}$$

© 2026 NSP
Natural Sciences Publishing Cor.

$$
\begin{aligned}
\beth_{5n} &= V_n(t) - V_{n-1}(t) = \frac{1-\varpi}{\Omega(\varpi)}\left\{\mathbb{A}_5\left(t, V_{n-1}(t)\right) - \mathbb{A}_5\left(t, V_{n-2}(t)\right)\right\},\\
\beth_{6n} &= S_{vn}(t) - S_{vn-1}(t) = \frac{1-\varpi}{\Omega(\varpi)}\left\{\mathbb{A}_6\left(t, S_{vn-1}(t)\right) - \mathbb{A}_6\left(t, S_{vn-2}(t)\right)\right\},\\
\beth_{7n} &= E_{vn}(t) - E_{vn-1}(t) = \frac{1-\varpi}{\Omega(\varpi)}\left\{\mathbb{A}_7\left(t, E_{vn-1}(t)\right) - \mathbb{A}_7\left(t, E_{vn-2}(t)\right)\right\},\\
\beth_{8n} &= I_{vn}(t) - I_{vn-1}(t) = \frac{1-\varpi}{\Omega(\varpi)}\left\{\mathbb{A}_8\left(t, I_{vn-1}(t)\right) - \mathbb{A}_8\left(t, I_{vn-2}(t)\right)\right\}.
\end{aligned} \tag{9}
$$

The norm of the sides and the triangle inequality lead to:

$$
\begin{aligned}
\|\beth_{1n}(t)\| &= \|S_n(t) - S_{n-1}(t)\| \le \frac{1-\varpi}{F(\varpi)}\left\|\mathbb{A}_1\left(t, S_{n-1}(t)\right) - \mathbb{A}_1\left(t, S_{n-2}(t)\right)\right\|\\
&\quad + \frac{\varpi}{\Omega(\varpi)\Gamma(\varpi)}\left\|\int_0^t \left\{\mathbb{A}_1\left(t, S_{n-1}(t)\right) - \mathbb{A}_1\left(t, S_{n-2}(t)\right)\right\}(t-\omega)^{\varpi-1}\,d\omega\right\|,\\
\|\beth_{2n}(t)\| &= \|E_n(t) - E_{n-1}(t)\| \le \frac{1-\varpi}{F(\varpi)}\left\|\mathbb{A}_2\left(t, E_{n-1}(t)\right) - \mathbb{A}_2\left(t, E_{n-2}(t)\right)\right\|\\
&\quad + \frac{\varpi}{\Omega(\varpi)\Gamma(\varpi)}\left\|\int_0^t \left\{\mathbb{A}_2\left(t, E_{n-1}(t)\right) - \mathbb{A}_2\left(t, E_{n-2}(t)\right)\right\}(t-\omega)^{\varpi-1}\,d\omega\right\|,\\
\|\beth_{3n}(t)\| &= \|I_n(t) - I_{n-1}(t)\| \le \frac{1-\varpi}{F(\varpi)}\left\|\mathbb{A}_3\left(t, I_{n-1}(t)\right) - \mathbb{A}_3\left(t, I_{n-2}(t)\right)\right\|\\
&\quad + \frac{\varpi}{\Omega(\varpi)\Gamma(\varpi)}\left\|\int_0^t \left\{\mathbb{A}_3\left(t, I_{n-1}(t)\right) - \mathbb{A}_3\left(t, I_{n-2}(t)\right)\right\}(t-\omega)^{\varpi-1}\,d\omega\right\|,\\
\|\beth_{4n}(t)\| &= \|R_n(t) - R_{n-1}(t)\| \le \frac{1-\varpi}{F(\varpi)}\left\|\mathbb{A}_4\left(t, R_{n-1}(t)\right) - \mathbb{A}_4\left(t, R_{n-2}(t)\right)\right\|\\
&\quad + \frac{\varpi}{\Omega(\varpi)\Gamma(\varpi)}\left\|\int_0^t \left\{\mathbb{A}_4\left(t, R_{n-1}(t)\right) - \mathbb{A}_4\left(t, R_{n-2}(t)\right)\right\}(t-\omega)^{\varpi-1}\,d\omega\right\|,\\
\|\beth_{5n}(t)\| &= \|V_n(t) - V_{n-1}(t)\| \le \frac{1-\varpi}{F(\varpi)}\left\|\mathbb{A}_5\left(t, V_{n-1}(t)\right) - \mathbb{A}_5\left(t, V_{n-2}(t)\right)\right\|\\
&\quad + \frac{\varpi}{\Omega(\varpi)\Gamma(\varpi)}\left\|\int_0^t \left\{\mathbb{A}_5\left(t, V_{n-1}(t)\right) - \mathbb{A}_5\left(t, V_{n-2}(t)\right)\right\}(t-\omega)^{\varpi-1}\,d\omega\right\|,\\
\|\beth_{6n}(t)\| &= \left\|S_{vn}(t) - S_{v(n-1)}(t)\right\| \le \frac{1-\varpi}{F(\varpi)}\left\|\mathbb{A}_6\left(t, S_{vn-1}(t)\right) - \mathbb{A}_6\left(t, S_{vn-2}(t)\right)\right\|\\
&\quad + \frac{\varpi}{\Omega(\varpi)\Gamma(\varpi)}\left\|\int_0^t \left\{\mathbb{A}_6\left(t, S_{vn-1}(t)\right) - \mathbb{A}_6\left(t, S_{vn-2}(t)\right)\right\}(t-\omega)^{\varpi-1}\,d\omega\right\|,\\
\|\beth_{7n}(t)\| &= \left\|E_{vn}(t) - E_{v(n-1)}(t)\right\| \le \frac{1-\varpi}{F(\varpi)}\left\|\mathbb{A}_7\left(t, E_{vn-1}(t)\right) - \mathbb{A}_7\left(t, E_{vn-2}(t)\right)\right\|\\
&\quad + \frac{\varpi}{\Omega(\varpi)\Gamma(\varpi)}\left\|\int_0^t \left\{\mathbb{A}_7\left(t, E_{vn-1}(t)\right) - \mathbb{A}_7\left(t, E_{vn-2}(t)\right)\right\}(t-\omega)^{\varpi-1}\,d\omega\right\|,\\
\|\beth_{8n}(t)\| &= \left\|I_{vn}(t) - I_{v(n-1)}(t)\right\| \le \frac{1-\varpi}{F(\varpi)}\left\|\mathbb{A}_8\left(t, I_{vn-1}(t)\right) - \mathbb{A}_8\left(t, I_{vn-2}(t)\right)\right\|\\
&\quad + \frac{\varpi}{\Omega(\varpi)\Gamma(\varpi)}\left\|\int_0^t \left\{\mathbb{A}_8\left(t, I_{vn-1}(t)\right) - \mathbb{A}_8\left(t, I_{vn-2}(t)\right)\right\}(t-\omega)^{\varpi-1}\,d\omega\right\|.
\end{aligned} \tag{10}
$$

Considering the following, since the kernel fulfills the Lipschitz condition:

$$
\begin{aligned}
\|\beth_{1n}(t)\| &\le \frac{1-\varpi}{F(\varpi)}\mathfrak{A}_1\|\beth_{1n-1}(t)\|\\
&\quad + \frac{\varpi}{\Omega(\varpi)\Gamma(\varpi)}\mathfrak{A}_1\int_0^t (t-\omega)^{\varpi-1}\|\beth_{1n-1}(t)\|d\omega,\\
\|\beth_{2n}(t)\| &\le \frac{1-\varpi}{F(\varpi)}\mathfrak{A}_2\|\beth_{2n-1}(t)\|
\end{aligned}
$$

© 2026 NSP
Natural Sciences Publishing Cor.

$$
\begin{aligned}
&+\frac{\varpi}{\Omega(\varpi)\Gamma(\varpi)}\mathfrak{A}_2\int_0^t(t-\omega)^{\varpi-1}\|\urcorner_{2n-1}(t)\|d\omega,\\
\|\urcorner_{3n}(t)\| &\leq \frac{1-\varpi}{F(\varpi)}\mathfrak{A}_3\|\urcorner_{3n-1}(t)\|\\
&+\frac{\varpi}{\Omega(\varpi)\Gamma(\varpi)}\mathfrak{A}_3\int_0^t(t-\omega)^{\varpi-1}\|\urcorner_{3n-1}(t)\|d\omega,\\
\|\urcorner_{4n}(t)\| &\leq \frac{1-\varpi}{F(\varpi)}\mathfrak{A}_4\|\urcorner_{4n-1}(t)\|\\
&+\frac{\varpi}{\Omega(\varpi)\Gamma(\varpi)}\mathfrak{A}_4\int_0^t(t-\omega)^{\varpi-1}\|\urcorner_{4n-1}(t)\|d\omega,\\
\|\urcorner_{5n}(t)\| &\leq \frac{1-\varpi}{F(\varpi)}\mathfrak{A}_5\|\urcorner_{5n-1}(t)\|\\
&+\frac{\varpi}{\Omega(\varpi)\Gamma(\varpi)}\mathfrak{A}_5\int_0^t(t-\omega)^{\varpi-1}\|\urcorner_{5n-1}(t)\|d\omega,\\
\|\urcorner_{6n}(t)\| &\leq \frac{1-\varpi}{F(\varpi)}\mathfrak{A}_6\|\urcorner_{6n-1}(t)\|\\
&+\frac{\varpi}{\Omega(\varpi)\Gamma(\varpi)}\mathfrak{A}_6\int_0^t(t-\omega)^{\varpi-1}\|\urcorner_{6n-1}(t)\|d\omega,\\
\|\urcorner_{7n}(t)\| &\leq \frac{1-\varpi}{F(\varpi)}\mathfrak{A}_7\|\urcorner_{7n-1}(t)\|\\
&+\frac{\varpi}{\Omega(\varpi)\Gamma(\varpi)}\mathfrak{A}_7\int_0^t(t-\omega)^{\varpi-1}\|\urcorner_{7n-1}(t)\|d\omega,\\
\|\urcorner_{8n}(t)\| &\leq \frac{1-\varpi}{F(\varpi)}\mathfrak{A}_8\|\urcorner_{8n-1}(t)\|\\
&+\frac{\varpi}{\Omega(\varpi)\Gamma(\varpi)}\mathfrak{A}_8\int_0^t(t-\omega)^{\varpi-1}\|\urcorner_{8n-1}(t)\|d\omega. \qquad (11)
\end{aligned}
$$

Thus, the proof of the theorem has been established.

Theorem 4.2. *(Existence of the solution): A solution exists for Equation (6) provided that the condition is identified. The value of t_{max} satisfies*

$$\frac{\mathfrak{A}_i}{\Omega(\varpi)}\left(1-\varpi+\frac{t_{max}^{\varpi}}{\Gamma(\varpi)}\right) \quad i\in\{1,2,3,\ldots,8\}.$$

Proof. Assume that the functions $S_h(t),E_h(t),I_h(t),V_h(t),R_h(t),S_v(t),E_v(t),I_v(t)$ are subject to constraints.

Equation (3) results in Equation (12).

$$
\begin{aligned}
\|\urcorner_{1n}(t)\| &\leq \|S(0)\|\left\{\frac{\mathfrak{A}_1}{\Omega(\varpi)}\left(1-\varpi+\frac{t_{\max}^{\varpi}}{\Gamma(\varpi)}\right)\right\},\\
\|\urcorner_{2n}(t)\| &\leq \|E(0)\|\left\{\frac{\mathfrak{A}_2}{\Omega(\varpi)}\left(1-\varpi+\frac{t_{\max}^{\varpi}}{\Gamma(\varpi)}\right)\right\},\\
\|\urcorner_{3n}(t)\| &\leq \|I(0)\|\left\{\frac{\mathfrak{A}_3}{\Omega(\varpi)}\left(1-\varpi+\frac{t_{\max}^{\varpi}}{\Gamma(\varpi)}\right)\right\},\\
\|\urcorner_{4n}(t)\| &\leq \|R(0)\|\left\{\frac{\mathfrak{A}_4}{\Omega(\varpi)}\left(1-\varpi+\frac{t_{\max}^{\varpi}}{\Gamma(\varpi)}\right)\right\},\\
\|\urcorner_{5n}(t)\| &\leq \|V(0)\|\left\{\frac{\mathfrak{A}_5}{\Omega(\varpi)}\left(1-\varpi+\frac{t_{\max}^{\varpi}}{\Gamma(\varpi)}\right)\right\},\\
\|\urcorner_{6n}(t)\| &\leq \|S_v(0)\|\left\{\frac{\mathfrak{A}_6}{\Omega(\varpi)}\left(1-\varpi+\frac{t_{\max}^{\varpi}}{\Gamma(\varpi)}\right)\right\},\\
\|\urcorner_{7n}(t)\| &\leq \|E_v(0)\|\left\{\frac{\mathfrak{A}_7}{\Omega(\varpi)}\left(1-\varpi+\frac{t_{\max}^{\varpi}}{\Gamma(\varpi)}\right)\right\},
\end{aligned}
$$

© 2026 NSP
Natural Sciences Publishing Cor.

$$\|\urcorner_{8n}(t)\| \leq \|I_v(0)\| \left\{ \frac{\mathfrak{A}_8}{\Omega(\varpi)} \left(1-\varpi+\frac{t_{\max}^{\varpi}}{\Gamma(\varpi)}\right)\right\}. \tag{12}$$

The functions $\urcorner_{1n}(t), \urcorner_{2n}(t), \urcorner_{3n}(t), \urcorner_{4n}(t), \urcorner_{5n}(t), \urcorner_{6n}(t), \urcorner_{7n}(t), \urcorner_{8n}(t)$ specified in Equation (12) exist and are smooth.

Moreover, to demonstrate that these functions satisfy Equation (12), it is assumed that

$$\begin{aligned}
S(t)-S(0) &= S_n(t)-\partial_{1n}(t),\\
E(t)-E(0) &= E_n(t)-\partial_{2n}(t),\\
I(t)-I(0) &= I_n(t)-\partial_{3n}(t),\\
R(t)-R(0) &= R_n(t)-\partial_{4n}(t),\\
V(t)-V(0) &= V_n(t)-\partial_{5n}(t),\\
S_v(t)-S_v(0) &= S_{vn}(t)-\partial_{6n}(t),\\
E_v(t)-E_v(0) &= E_{vn}(t)-\partial_{7n}(t),\\
I_v(t)-I_v(0) &= I_{vn}(t)-\partial_{8n}(t).
\end{aligned} \tag{13}$$

for $\partial_{1n}, \partial_{2n}, \partial_{3n}, \partial_{4n}, \partial_{5n}, \partial_{6n}, \partial_{7n}, \partial_{8n}$.

$$\begin{aligned}
&\left\|\partial_{1(\infty)}(t)\right\| \to 0, \quad \left\|\partial_{2(\infty)}(t)\right\| \to 0, \quad \left\|\partial_{3(\infty)}(t)\right\| \to 0,\\
&\left\|\partial_{4(\infty)}(t)\right\| \to 0, \quad \left\|\partial_{5(\infty)}(t)\right\| \to 0, \quad \left\|\partial_{6(\infty)}(t)\right\| \to 0,\\
&\left\|\partial_{7(\infty)}(t)\right\| \to 0, \quad \left\|\partial_{8(\infty)}(t)\right\| \to 0.
\end{aligned}$$

Thus, for the term $\partial_{1n}(t)$, we have:

$$\begin{aligned}
&\|\urcorner_{1n}(t)\| \leq \tfrac{1-\varpi}{F(\varpi)} \left\|\mathbb{A}_1\left(t,S(t)\right)-\mathbb{A}_1\left(t,S_{n-1}(t)\right)\right\|\\
&+\tfrac{\varpi}{\Omega(\varpi)\Gamma(\varpi)}\\
&\left\|\int_0^t \left((t-\omega)^{\varpi-1}\right) \mathbb{A}_1\left(t,S(\omega)\right)-\mathbb{A}_1\left(t,S_{n-1}(\omega)\right) d\omega\right\|\\
&\leq \tfrac{\mathfrak{A}_1}{\Omega(\varpi)} \left(1-\varpi+\tfrac{t_{\max}^{\varpi}}{\Gamma(\varpi)}\right) \|S(t)-S_{n-1}(t)\|
\end{aligned}$$

$$\|\urcorner_{1n}(t)\| \leq \pi \left\{ \frac{\mathfrak{A}_1}{\Omega(\varpi)} \left(1-\varpi+\frac{t_{\max}^{\varpi}}{\Gamma(\varpi)}\right)\right\}^{n+1}$$

where $\pi = \|S(t)-S_{n-1}(t)\|$. The analogous corrected bound applies for $\urcorner_{2n}$ through $\urcorner_{8n}$, each with its own kernel constant $\mathfrak{A}_2,\ldots,\mathfrak{A}_8$ in place of $\mathfrak{A}_1$.

Finally,

$$\left\|\partial_{j(\infty)}(t)\right\| \to 0, \quad j=\{1,2,3,4,5,6,7,8\}.$$

4.1 Computational Methods: Experiment and Approximation Techniques

This section discusses the computational methods used in the study, including the simulation approach and approximation techniques applied to the zika virus model described in Equation (3). The model, incorporating the initial conditions, features a nonlinear term *SI*. By applying the Laplace transform, the behavior of this term is analyzed further.

$$\begin{aligned}
\frac{\Omega(\varpi)}{1-\varpi}\frac{W^{\upsilon}L\{S(t)\}}{W^{\upsilon}+\frac{\varpi}{1-\varpi}} &= \frac{W^{\upsilon-1}S(0)}{W^{\upsilon}+\frac{\varpi}{1-\varpi}} + L\left\{\Pi-\beta S\frac{I_v}{N_v}-(\nu+\mu)S\right\},\\
\frac{\Omega(\varpi)}{1-\varpi}\frac{W^{\upsilon}L\{E(t)\}}{W^{\upsilon}+\frac{\varpi}{1-\varpi}} &= \frac{W^{\upsilon-1}E(0)}{W^{\upsilon}+\frac{\varpi}{1-\varpi}} + L\left\{\beta S\frac{I_v}{N_v}-(\sigma+\mu+\delta)E\right\},\\
\frac{\Omega(\varpi)}{1-\varpi}\frac{W^{\upsilon}L\{I(t)\}}{W^{\upsilon}+\frac{\varpi}{1-\varpi}} &= \frac{W^{\upsilon-1}I(0)}{W^{\upsilon}+\frac{\varpi}{1-\varpi}} + L\{\sigma E-(\gamma+\mu+\delta)I\},\\
\frac{\Omega(\varpi)}{1-\varpi}\frac{W^{\upsilon}L\{R(t)\}}{W^{\upsilon}+\frac{\varpi}{1-\varpi}} &= \frac{W^{\upsilon-1}R(0)}{W^{\upsilon}+\frac{\varpi}{1-\varpi}} + L\{\gamma I-\mu R\},
\end{aligned}$$

© 2026 NSP
Natural Sciences Publishing Cor.

$$\begin{aligned}
\frac{\Omega(\varpi)}{1-\varpi}\frac{W^{\mho}L\{V(t)\}}{W^{\mho}+\frac{\varpi}{1-\varpi}} &= \frac{W^{\mho-1}V(0)}{W^{\mho}+\frac{\varpi}{1-\varpi}} + L\{\nu S-\mu V\},\\
\frac{\Omega(\varpi)}{1-\varpi}\frac{W^{\mho}L\{S_v(t)\}}{W^{\mho}+\frac{\varpi}{1-\varpi}} &= \frac{W^{\mho-1}S_v(0)}{W^{\mho}+\frac{\varpi}{1-\varpi}} + L\left\{\Lambda_v(t)-\beta_v S_v\frac{I}{N}-\mu_v S_v\right\},\\
\frac{\Omega(\varpi)}{1-\varpi}\frac{W^{\mho}L\{E_v(t)\}}{W^{\mho}+\frac{\varpi}{1-\varpi}} &= \frac{W^{\mho-1}E_v(0)}{W^{\mho}+\frac{\varpi}{1-\varpi}} + L\left\{\beta_v S_v\frac{I}{N}-(\sigma_v+\mu_v)E_v\right\},\\
\frac{\Omega(\varpi)}{1-\varpi}\frac{W^{\mho}L\{I_v(t)\}}{W^{\mho}+\frac{\varpi}{1-\varpi}} &= \frac{W^{\mho-1}I_v(0)}{W^{\mho}+\frac{\varpi}{1-\varpi}} + L\{\sigma_v E_v-\mu_v I_v\}.
\end{aligned} \tag{14}$$

By rearranging, we obtain

$$\begin{aligned}
L\{S(t)\} &= \frac{S(0)}{W}+\frac{W^{\mho}(1-\mho)+\mho}{W^{\mho}(F(\mho))}L\left\{\Pi-\beta S\frac{I_v}{N_v}-(\nu+\mu)S\right\},\\
L\{E(t)\} &= \frac{E(0)}{W}+\frac{W^{\mho}(1-\mho)+\mho}{W^{\mho}(F(\mho))}L\left\{\beta S\frac{I_v}{N_v}-(\sigma+\mu+\delta)E\right\},\\
L\{I(t)\} &= \frac{I(0)}{W}+\frac{W^{\mho}(1-\mho)+\mho}{W^{\mho}(F(\mho))}L\{\sigma E-(\gamma+\mu+\delta)I\},\\
L\{R(t)\} &= \frac{R(0)}{W}+\frac{W^{\mho}(1-\mho)+\mho}{W^{\mho}(F(\mho))}L\{\gamma I-\mu R\},\\
L\{V(t)\} &= \frac{V(0)}{W}+\frac{W^{\mho}(1-\mho)+\mho}{W^{\mho}(F(\mho))}L\{\nu S-\mu V\},\\
L\{S_v(t)\} &= \frac{S_v(0)}{W}+\frac{W^{\mho}(1-\mho)+\mho}{W^{\mho}(F(\mho))}L\left\{\Lambda_v(t)-\beta_v S_v\frac{I}{N}-\mu_v S_v\right\},\\
L\{E_v(t)\} &= \frac{E_v(0)}{W}+\frac{W^{\mho}(1-\mho)+\mho}{W^{\mho}(F(\mho))}L\left\{\beta_v S_v\frac{I}{N}-(\sigma_v+\mu_v)E_v\right\},\\
L\{I_v(t)\} &= \frac{I_v(0)}{W}+\frac{W^{\mho}(1-\mho)+\mho}{W^{\mho}(F(\mho))}L\{\sigma_v E_v-\mu_v I_v\}.
\end{aligned} \tag{15}$$

Furthermore, applying the inverse Laplace transform to Equation (15) results in

$$\begin{aligned}
S(t) &= S(0)+L^{-1}\left[\left(\frac{W^{\mho}(1-\mho)+\mho}{W^{\mho}(F(\mho))}\right)L\left\{\Pi-\beta S\frac{I_v}{N_v}-(\nu+\mu)S\right\}\right],\\
E(t) &= E(0)+L^{-1}\left[\left(\frac{W^{\mho}(1-\mho)+\mho}{W^{\mho}(F(\mho))}\right)L\left\{\beta S\frac{I_v}{N_v}-(\sigma+\mu+\delta)E\right\}\right],\\
I(t) &= I(0)+L^{-1}\left[\left(\frac{W^{\mho}(1-\mho)+\mho}{W^{\mho}(F(\mho))}\right)L\{\sigma E-(\gamma+\mu+\delta)I\}\right],\\
R(t) &= R(0)+L^{-1}\left[\left(\frac{W^{\mho}(1-\mho)+\mho}{W^{\mho}(F(\mho))}\right)L\{\gamma I-\mu R\}\right],\\
V(t) &= V(0)+L^{-1}\left[\left(\frac{W^{\mho}(1-\mho)+\mho}{W^{\mho}(F(\mho))}\right)L\{\nu S-\mu V\}\right],\\
S_v(t) &= S_v(0)+L^{-1}\left[\left(\frac{W^{\mho}(1-\mho)+\mho}{W^{\mho}(F(\mho))}\right)L\left\{\Lambda_v(t)-\beta_v S_v\frac{I}{N}-\mu_v S_v\right\}\right],\\
E_v(t) &= E_v(0)+L^{-1}\left[\left(\frac{W^{\mho}(1-\mho)+\mho}{W^{\mho}(F(\mho))}\right)L\left\{\beta_v S_v\frac{I}{N}-(\sigma_v+\mu_v)E_v\right\}\right],\\
I_v(t) &= I_v(0)+L^{-1}\left[\left(\frac{W^{\mho}(1-\mho)+\mho}{W^{\mho}(F(\mho))}\right)L\{\sigma_v E_v-\mu_v I_v\}\right].
\end{aligned} \tag{16}$$

The method produces series solutions, which are given by

© 2026 NSP
Natural Sciences Publishing Cor.

$$\begin{aligned} S &= \sum_{y=0}^{\infty} S_y, \quad E = \sum_{y=0}^{\infty} E_y, \quad I = \sum_{y=0}^{\infty} I_y, \quad V = \sum_{y=0}^{\infty} V_y, \quad R = \sum_{y=0}^{\infty} R_y, \\ S_v &= \sum_{y=0}^{\infty} S_{vy}, \quad E_v = \sum_{y=0}^{\infty} E_{vy}, \quad I_v = \sum_{y=0}^{\infty} I_{vy}. \end{aligned} \tag{17}$$

By applying the initial condition, we obtain

$$\begin{aligned} S_{y+1}(t) &= S_y(0) + L^{-1}\left[\left(\frac{W^{\mho}(1-\mho)+\mho}{W^{\mho}(F(\mho))}\right) L\left\{\Pi - \beta S_y \frac{I_{vy}}{N_{vy}} - (\nu+\mu)S_y\right\}\right], \\ E_{y+1}(t) &= E_y(0) + L^{-1}\left[\left(\frac{W^{\mho}(1-\mho)+\mho}{W^{\mho}(F(\mho))}\right) L\left\{\beta S_y \frac{I_{vy}}{N_{vy}} - (\sigma+\mu+\delta)E_y\right\}\right], \\ I_{y+1}(t) &= I_y(0) + L^{-1}\left[\left(\frac{W^{\mho}(1-\mho)+\mho}{W^{\mho}(F(\mho))}\right) L\left\{\sigma E_y - (\gamma+\mu+\delta)I_y\right\}\right], \\ R_{y+1}(t) &= R_y(0) + L^{-1}\left[\left(\frac{W^{\mho}(1-\mho)+\mho}{W^{\mho}(F(\mho))}\right) L\left\{\gamma I_y - \mu R_y\right\}\right], \\ V_{y+1}(t) &= V_y(0) + L^{-1}\left[\left(\frac{W^{\mho}(1-\mho)+\mho}{W^{\mho}(F(\mho))}\right) L\left\{\nu S_y - \mu V_y\right\}\right], \\ S_{vy+1}(t) &= S_{vy}(0) + L^{-1}\left[\left(\frac{W^{\mho}(1-\mho)+\mho}{W^{\mho}(F(\mho))}\right) L\left\{\Lambda_{vy}(t) - \beta_{vy} S_{vy} \frac{I_y}{N_y} - \mu_{vy} S_{vy}\right\}\right], \\ E_{vy+1}(t) &= E_{vy}(0) + L^{-1}\left[\left(\frac{W^{\mho}(1-\mho)+\mho}{W^{\mho}(F(\mho))}\right) L\left\{\beta_{vy} S_{vy} \frac{I_y}{N_y} - (\sigma_{vy}+\mu_{vy})E_{vy}\right\}\right], \\ I_{vy+1}(t) &= I_{vy}(0) + L^{-1}\left[\left(\frac{W^{\mho}(1-\mho)+\mho}{W^{\mho}(F(\mho))}\right) L\left\{\sigma_{vy} E_{vy} - \mu_{vy} I_{vy}\right\}\right]. \end{aligned} \tag{18}$$

where $S_o(t) = S(0)$, $E_o(t) = E(0)$, $I_o(t) = I(0)$, $R_o(t) = R(0)$, $V_o(t) = V(0)$, $S_{\text{vo}}(t) = S_v(0)$, $E_o(t) = E_v(0)$, $I_{vo}(t) = I_v(0)$.

As n approaches infinity, it is expected that the approximate solution will be reached:

$$\begin{aligned} S(t) &= \lim_{y\to\infty} S_y(t), \quad E(t) = \lim_{y\to\infty} E_y(t), \quad I(t) = \lim_{y\to\infty} I_y(t), \\ R(t) &= \lim_{y\to\infty} R_y(t), \quad V(t) = \lim_{y\to\infty} V_y(t), \\ S_v(t) &= \lim_{y\to\infty} S_{vy}(t), \quad E_v(t) = \lim_{y\to\infty} E_{vy}(t), \quad I_v(t) = \lim_{y\to\infty} I_{vy}(t). \end{aligned} \tag{19}$$

4.2 Computational Experiment and Discussion

Computational experiments are crucial tools for investigating complex systems that are challenging to analyse using analytical methods alone. Using computational techniques and algorithms, these experiments allow for the modelling, simulation, and analysis of a wide range of physical and theoretical scenarios. In this section, the parameters used are $\Pi = 0.0391389432, \beta = 0.003, \nu = 0.5, \mu = 0.00003913894325, \sigma = 0.2, \delta = 0.001, \gamma = 0.166666667, \Lambda_v = 476.19047619, \beta_v = 0.003, \mu_v = 0.0476190476, \sigma_v = 0.1$ all are from [27,28] and the initial conditions for all variables are $S = 3320, E = 220, I = 100, R = 50, V = 1430, S_v = 9500, E_v = 600, I_v = 170$ also from [29], which are essential for accurate simulations.

5 Numerical Simulations and Discussion

Figure 2 shows fractional differentiation shortening the period of human susceptibility relative to the classical case, with the susceptible pool shrinking faster as α increases and the system growing correspondingly more sensitive to

© 2026 NSP
Natural Sciences Publishing Cor.

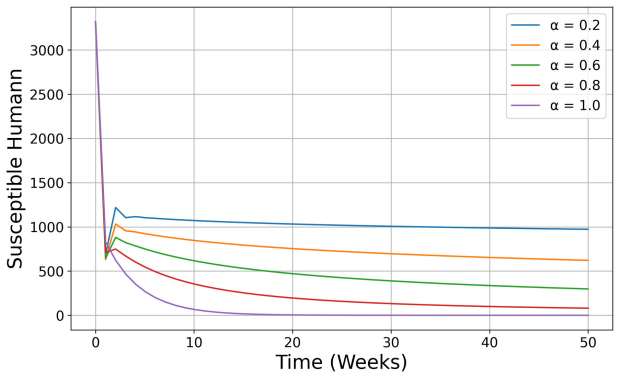


Fig. 2: Impact of fractional-order on susceptible human

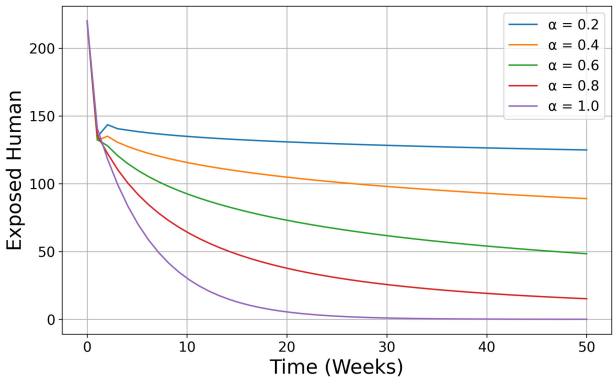


Fig. 3: Impact of fractional-order on Exposed human

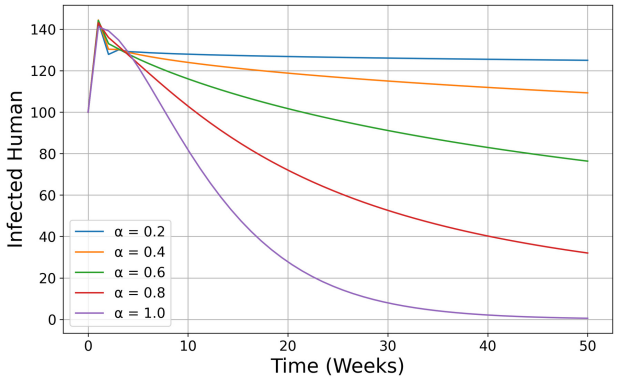


Fig. 4: Impact of fractional-order on Infected human

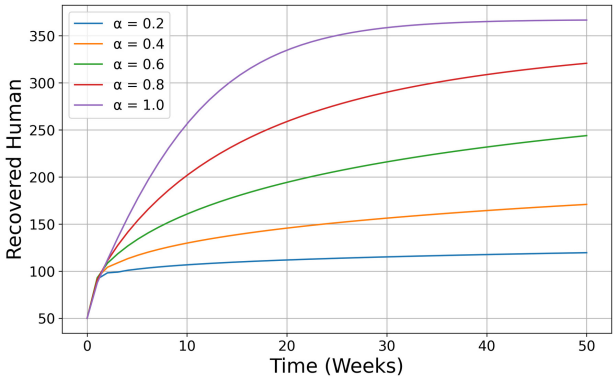


Fig. 5: Impact of fractional-order on Recovered human

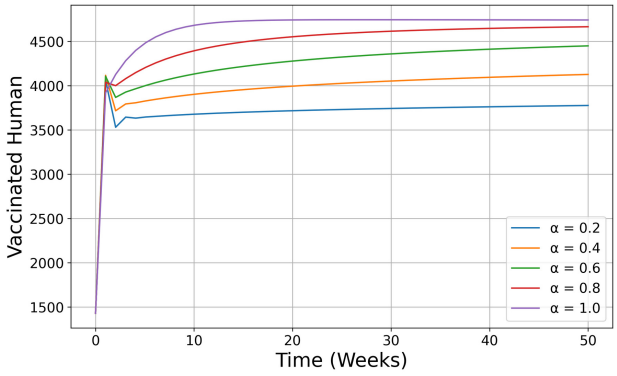


Fig. 6: Impact of fractional-order on Vaccinated human

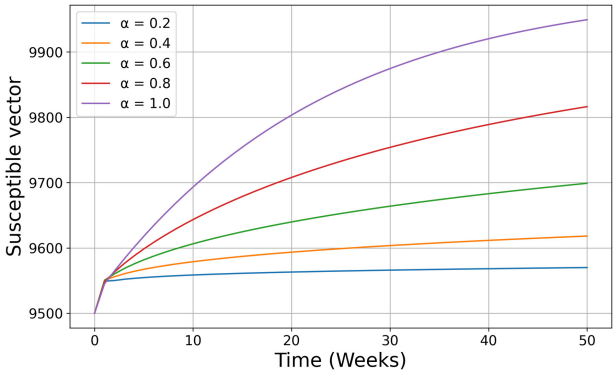


Fig. 7: Impact of fractional-order on Susceptible vector

transmission-rate changes. The exposed-class trajectory in Figure 3 shows the same pattern from the other side: the fractional model resolves early epidemic waves and stabilisation trends that the integer-order case smooths over, yielding a slower cumulative-case trajectory overall. Read together with the infected- and recovered-class results in Figures 4 and 5, a consistent picture emerges across α: at $\alpha = 0.2$–0.4 the epidemic is large but slow-moving, leaving time for interventions such as vaccination and contact tracing; at $\alpha = 0.6$–0.8 progression and recovery both accelerate, favouring faster-cycle responses such as active case-finding and isolation; and at $\alpha = 1.0$, the classical limit, the outbreak moves quickly enough to demand immediate measures: mass vaccination, quarantine, and surge capacity in health services, before the system is overwhelmed.

The vaccinated and vector compartments follow the same α-dependence. Figure 6 shows vaccination coverage building fastest at higher α, where sustaining momentum and equitable distribution matters more than the initial scale-up effort that lower α demands; the mosquito compartments in Figures 7 and 8 mirror this, with the susceptible and infected vector

© 2026 NSP
Natural Sciences Publishing Cor.

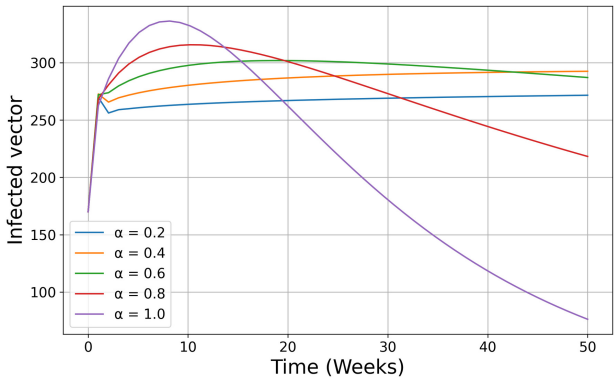


Fig. 8: Impact of fractional-order on Infected vector

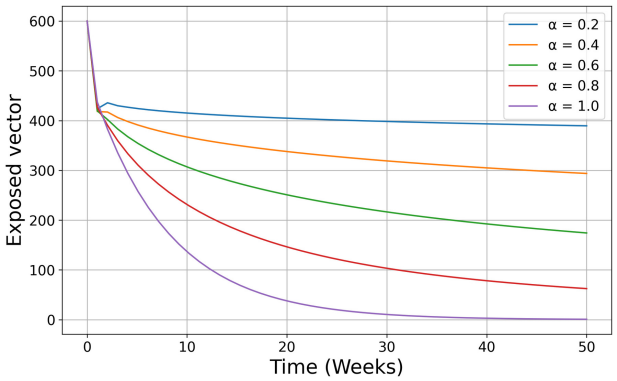


Fig. 9: Impact of fractional-order on Exposed vector

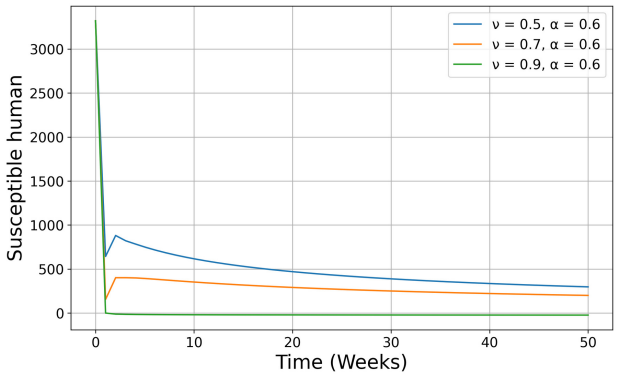


Fig. 10: Impact of vaccination rate on susceptible humans when $\alpha = 0.6$

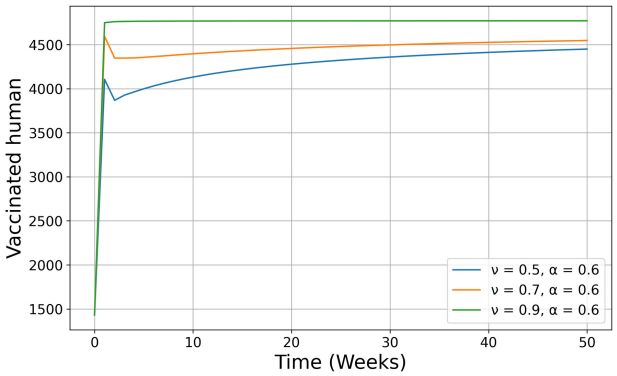


Fig. 11: Impact of vaccination rate on Vaccinated human when $\alpha = 0.6$

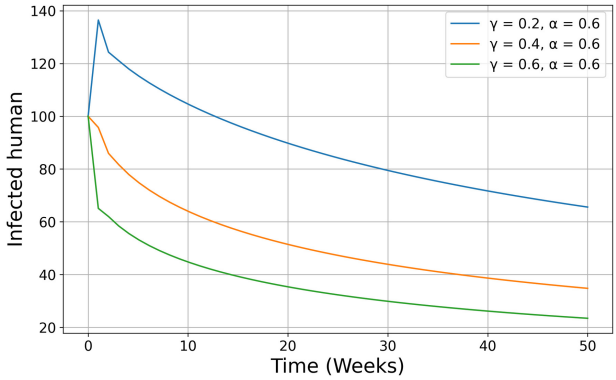


Fig. 12: Impact of treatment rate on Infected human when $\alpha = 0.6$

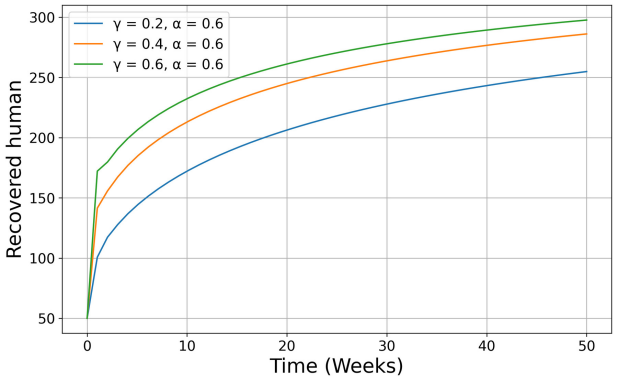


Fig. 13: Impact of treatment rate on Recovered human when $\alpha = 0.6$

© 2026 NSP
Natural Sciences Publishing Cor.

populations both growing more rapidly as $\alpha \to 1$, an argument for front-loading vector-control effort rather than treating it as a constant-rate background activity. Figure 9 runs the other way: the exposed vector population is *largest* at low α, where slower per-capita exposure is offset by a longer residence time in the exposed class, so a low fractional order should not be read as a low-priority signal for vector control aimed at this compartment.

Figures 10–11 and 12–13 turn from the fractional order to the two interventions directly, at fixed $\alpha = 0.6$. Raising the vaccination rate ν depletes the susceptible class and builds the vaccinated class in tandem, consistent with the vaccination threshold derived in Section 3.4; raising the recovery rate γ depletes the infected class and builds the recovered class the same way. Both results are the numerical counterpart of the sensitivity signs already reported in Table 3; ν and γ each carry a negative sensitivity index for R_0, and together they indicate that vaccination scale-up and faster case recovery are the two levers with the most direct numerical effect on bringing the simulated epidemic under control.

6 Conclusion

This study developed an Atangana-Baleanu-Caputo (ABC) fractional-order model of Zika virus transmission that couples human (S,E,I,R,V) and mosquito (S_v,E_v,I_v) dynamics with vaccination and early-detection interventions. The disease-free equilibrium is locally asymptotically stable whenever the basic reproduction number

$$R_0 = \sqrt{\frac{\beta\beta_v\mu\sigma\sigma_v}{(\nu+\mu)(\sigma+\mu+\delta)(\gamma+\mu+\delta)(\sigma_v+\mu_v)\mu_v}}$$

falls below unity, and an endemic equilibrium exists and is biologically feasible whenever $R_0 > 1$. The vaccination threshold analysis established that transmission is interrupted once $\nu > \mu(R_0 - 1)$, corresponding to a critical vaccination coverage of $p_v^{\text{crit}} = 1 - 1/R_0$; for the baseline parameter set used in the simulations ($R_0 = 3$), at least 66.7% coverage is required. The normalised sensitivity analysis (Table 3) identified the human-to-mosquito and mosquito-to-human transmission rates β and β_v, and the mosquito progression rate σ_v, as the parameters that increase R_0 most strongly, while the vaccination rate ν, the recovery rate γ, and the natural and disease-induced mortality rates μ and δ act to reduce it, indicating that vaccination scale-up and faster case recovery are the interventions with the greatest leverage over disease persistence.

Incorporating the ABC fractional derivative changed these dynamics substantially: as shown in Figures 2–9, lower fractional orders ($\alpha = 0.2, 0.4$) produced slower depletion of the susceptible population and a more persistent, elevated exposed/infectious class over the 50-week simulation horizon, consistent with the memory effect of the ABC operator prolonging transmission relative to the classical integer-order case ($\alpha = 1.0$). This confirms that the fractional-order formulation captures a more gradual, sustained epidemic profile than integer-order models, with direct implications for how long vaccination and detection efforts must be sustained to achieve control. Future research will strengthen transmission models by incorporating time-dependent and stochastic factors, validating results with real-world data, and developing more effective quarantine and vaccination strategies. Ongoing simulations will focus on improving fractional-order models and examining host-reservoir interactions.

Specifically, the next phase will involve optimal control analysis of the proposed fractional-order model, utilising advanced optimisation techniques to identify the most cost-effective and efficient intervention strategies, following the optimal control and cost-effectiveness analyses used for Ebola virus disease [25] and for illicit drug use and banditry [26]. This approach will balance vaccination, isolation, and public health measures to minimise both disease spread and economic impact. The expected results will provide actionable insights to help policymakers design targeted, efficient-resource Zika virus control strategies. The model incorporates the Atangana-Baleanu-Caputo fractional derivatives to capture the memory effects of disease transmission. It ensures positivity, stability, and solution uniqueness, as confirmed by fixed-point theory and Lipschitz conditions. We derive semi-analytical solutions using the Laplace Adomian Decomposition Method.

Statements and Declarations

Ethics approval

Not applicable

Consent to participate

Not applicable

© 2026 NSP
Natural Sciences Publishing Cor.

Consent for publication

Not applicable

Data Availability

Datasets were not generated or analysed during the current study.

Competing interests

The authors have no competing interests to disclose regarding this work.

Funding

This work was partially supported by a grant from the IMU-CDC and Simons Foundation.

Acknowledgements

The authors hereby acknowledge everyone who has contributed to the success of this research work.

References

[1] N. Gyawali, R. S. Bradbury and A. W. Taylor-Robinson, The global spread of Zika virus: is public and media concern justified in regions currently unaffected, *Infect. Dis. Poverty* **5**, Article 37 (2016). doi:10.1186/s40249-016-0132-y.
[2] A. A. Al-Qahtani, N. Nazir, M. R. Al-Anazi, S. Rubino and M. N. Al-Ahdal, Zika virus: a new pandemic threat, *J. Infect. Dev. Ctries.* **10**(3), 201–207 (2016). doi:10.3855/jidc.8350.
[3] R. K. Gilbert, L. R. Petersen, M. A. Honein, C. A. Moore and S. A. Rasmussen, Zika virus as a cause of birth defects: were the teratogenic effects of Zika virus missed for decades?, *Birth Defects Res.* **115**(3), 265–274 (2023). doi:10.1002/bdr2.2134.
[4] T. Adebanjo, S. Godfred-Cato, L. Viens, M. Fischer, J. E. Staples, W. Kuhnert-Tallman and C. A. Moore, Update: interim guidance for the diagnosis, evaluation, and management of infants with possible congenital Zika virus infection — United States, October 2017, *MMWR Morb. Mortal. Wkly. Rep.* **66**(41), 1089–1099 (2017). doi:10.15585/mmwr.mm6641a1.
[5] P. Sampathkumar and J. L. Sanchez, Zika virus in the Americas: a review for clinicians, *Mayo Clin. Proc.* **91**(4), 514–521 (2016). doi:10.1016/j.mayocp.2016.02.017.
[6] M. J. Keeling and P. Rohani, *Modeling Infectious Diseases in Humans and Animals*, Princeton University Press, 2008.
[7] W. O. Kermack and A. G. McKendrick, A contribution to the mathematical theory of epidemics, *Proc. R. Soc. Lond. A* **115**(772), 700–721 (1927).
[8] B. D. Foy, K. C. Kobylinski, J. L. Chilson Foy, B. J. Blitvich, A. Travassos da Rosa, A. D. Haddow, R. S. Lanciotti and R. B. Tesh, Probable non-vector-borne transmission of Zika virus, Colorado, USA, *Emerg. Infect. Dis.* **17**(5), 880–882 (2011). doi:10.3201/eid1705.101939.
[9] C. W. Chukwu, C. E. Madubueze, M. O. Nnakwe, J. O. Akanni, Z. Chazuka and Fatmawati, Mathematical analysis and numerical simulation of campylobacteriosis dynamics: assessing the roles of house flies and contaminated food products as mechanical vectors, *J. Biosaf. Biosecur.* **8**(2), 91–110 (2026). doi:10.1016/j.jobb.2026.03.005.
[10] F. B. Agusto, S. Bewick and W. F. Fagan, Mathematical model of Zika virus with vertical transmission, *Infect. Dis. Model.* **2**(2), 244–267 (2017). doi:10.1016/j.idm.2017.05.003.
[11] A. Bangia and R. Bhardwaj, Fractional ordered epidemiology model simulation for pathogenesis of the pandemic, *Franklin Open* **12**, 100320 (2025). doi:10.1016/j.fraope.2025.100320.
[12] Y. Chen, F. Liu, Q. Yu and T. Li, Review of fractional epidemic models, *Appl. Math. Model.* **97**, 281–307 (2021). doi:10.1016/j.apm.2021.03.044.
[13] T. Alinei-Poiana, E. H. Dulf and L. Kovacs, Fractional calculus in mathematical oncology, *Sci. Rep.* **13**, 10083 (2023). doi:10.1038/s41598-023-37196-9.
[14] Atangana, A. and Baleanu, D. (2016) New Fractional Derivatives with Nonlocal and Non-Singular Kernel: Theory and Applications to Heat Transfer Model. Thermal Science, 20, 763-769. https://doi.org/10.2298/TSCI160111018A
[15] S. Rashid, F. Jarad and A. G. Ahmad, A novel fractal-fractional order model for the understanding of an oscillatory and complex behavior of human liver with non-singular kernel, *Results Phys.* **35**, 105292 (2022). doi:10.1016/j.rinp.2022.105292.

© 2026 NSP
Natural Sciences Publishing Cor.

[16] A. Omame, M. Abbas and C. P. Onyenegecha, A fractional-order model for COVID-19 and tuberculosis co-infection using Atangana–Baleanu derivative, *Chaos Solitons Fractals* **153**(1), 111486 (2021). doi:10.1016/j.chaos.2021.111486.
[17] M. Farman, A. Akgül, S. Askar, T. Botmart, A. Ahmad and H. Ahmad, Modeling and analysis of fractional order Zika model, *AIMS Math.* **7**(3), 3912–3938 (2022). doi:10.3934/math.2022216.
[18] O. Sharomi and T. Malik, Optimal control in epidemiology, *Ann. Oper. Res.* **251**, 55–71 (2017). doi:10.1007/s10479-015-1834-4.
[19] Y. Zhou, J. Wu and M. Wu, Optimal isolation strategies of emerging infectious diseases with limited resources, *Math. Biosci. Eng.* **10**(5&6), 1691–1701 (2013). doi:10.3934/mbe.2013.10.1691.
[20] S. Ajao, J. O. Akanni, T. Akinwumi, M. A. Omoloye, I. Olopade and O. A. Odebiyi, A mathematical approach to malaria eradication: insights from vaccine strategies, *J. Prime Res. Math.*, 41–67 (2026).
[21] J. O. Akanni, S. Ajao and Fatmawati, Mathematical modelling of the dengue transmission, focusing on the imperfect vaccination, waning immunity and control, *Franklin Open* (2026).
[22] M. Bouziane, S. Bercisse, A. Chekroun and S. Girel, How delay, isolation and vaccination shape epidemic waves: a bifurcation approach in mathematical epidemiology, arXiv:2603.24107 [math.DS] (2026).
[23] D. Klinkenberg, C. Fraser and H. Heesterbeek, The effectiveness of contact tracing in emerging epidemics, *PLoS ONE* **1**(1), e12 (2006). doi:10.1371/journal.pone.0000012.
[24] T. Y. Miyaoka, J. F. C. A. Meyer and S. Lenhart, Multiple optimal control strategies in a vector-borne reaction-diffusion model, *Proc. Ser. Braz. Soc. Comput. Appl. Math.* **6**(2) (2018). doi:10.5540/03.2018.006.02.0304.
[25] S. Ajao, J. O. Akanni, N. K. D. O. Opoku, D. Enegesele and C. E. Madubueze, Optimal control and cost-effectiveness analysis of Ebola virus disease dynamics in a population, *Iran. J. Sci.* (2026), advance online publication. doi:10.1007/s40995-026-01992-5.
[26] A. Abidemi and J. O. Akanni, Dynamics of illicit drug use and banditry population with optimal control strategies and cost-effectiveness analysis, *Comput. Appl. Math.* **41**, Article 53 (2022). doi:10.1007/s40314-022-01760-2.
[27] Centre for Disease Prevention and Control, Symptoms, diagnosis and treatment: Zika virus (2016). https://www.cdc.gov/zika/symptoms/index.html.
[28] C. J. Silva and D. F. M. Torres, An optimal control approach to malaria prevention via insecticide-treated nets, *Conf. Pap. Math.* **2013**, Article ID 658468 (2013). doi:10.1155/2013/658468.
[29] S. Usman, I. Isa Adamu and H. Babando, Mathematical model for the transmission dynamics of Zika virus infection with combined vaccination and treatment interventions, *J. Appl. Math. Phys.* **5**, 1964–1978 (2017). doi:10.4236/jamp.2017.510166.

© 2026 NSP
Natural Sciences Publishing Cor.